IEEE Access
Multidisciplinary | Rapid Review | Open Access Journal

Received December 6, 2020, accepted December 20, 2020, date of publication December 23, 2020, date of current version January 4, 2021.

Digital Object Identifier 10.1109/ACCESS.2020.3046920

Bandwidth Enhancement for Wireless Power Transfer System Employing Non-Linear Resonator

XU YANG[1,2], CHAOQUN JIAO[1], JUNFENG YANG[1], JING FAN[3], DINGZHEN LI[3], AND BAO WANG[3]

[1]School of Electrical Engineering, Beijing Jiaotong University, Beijing 100044, China
[2]School of Intelligent Manufacturing, Nanyang Institute of Technology, Nanyang 473004, China
[3]School of Information Engineering, Nanyang Institute of Technology, Nanyang 473004, China

Corresponding authors: Chaoqun Jiao (chqjiao@bjtu.edu.cn) and Jing Fan (fanjing@nyist.edu.cn)

This work was supported in part by the National Natural Science Foundation of China under Grant 12004202, in part by the Fundamental Research Funds for the Central Universities under Grant 2019YJS168, in part by the Research and Development Special Funding Projects of Henan Science and Technology Department under Grant 192102210071, and in part by the Key Scientific Research Project of Henan Provincial Education Department under Grant 21A470004.

ABSTRACT In order to enhance the tolerance of frequency misalignment and solve the amplitude-bandwidth limitation issue of the traditional linear resonance wireless power transfer (WPT) system, this paper proposes a non-linear resonance WPT (NLR-WPT) system which is mainly composed of high frequency power supply, primary linear resonator, secondary non-linear resonator, and load. Such non-linear resonator can be implemented with passive linear capacitor and magnetic saturation inductor, and it can be described by Duffing equation. It has been shown that the bandwidth of NLR-WPT system in the nonlinear state is 1.7 times larger than that in the linear state. In addition, the output voltage basically stabilizes at the same level, the voltage fluctuation is less than 5% over the power frequency ranging from 25.6 kHz to 31.8 kHz, and high overall efficiency of 86.5% can be achieved under a wide range of frequency (27.5 kHz-30.1 kHz). Furthermore, the range of frequency can be extended significantly over which the output voltage is maintained even while the compensate capacitance, load, or coupling coefficient values vary in a certain range. The experimental results agree well with the theoretical analysis and verify the validity of the NLR-WPT system with non-linear resonator. This paper provides a simple and effective scheme to suppress the fluctuation of output voltage, which is suitable for the applications of constant voltage charging such as moving devices or electric vehicles.

INDEX TERMS Wireless power transfer (WPT), bandwidth enhancement, stable output voltage, non-linear resonance, magnetic saturation inductor, Duffing equation.

I. INTRODUCTION

Magnetically coupled resonance (MCR) wireless power transfer (WPT) has now grown from a fledgling technology to an alternative technology for domestic and industrial applications [1], [2]. By means of its excellent characteristics of non-contact, full sealing, convenience and automation, the MCR-WPT technique has been taken as an ideal technical solution for electric vehicles, portable electronic products, household appliances, robotics and other fields [3], [4].

Energy is transferred between the primary linear resonator and secondary linear resonator of MCR-WPT system according to the principle of electromagnetic induction and magnetic resonance [5]. The typical block diagram of the MCR-WPT system is shown in Fig. 1. The primary linear resonator is driven by a high-frequency power supply, while the magnetic energy is transmitted from primary linear resonator to the secondary linear resonator through time-varying magnetic fields. Subsequently, the received high frequency AC is converted to DC by way of a rectifier and a filter before it is delivered to a load, which is often a rechargeable battery [6]. Both the primary linear resonator and the secondary linear resonator are composed of compensation network and coil, which is the key to the MCR-WPT system [7]. The transfer efficiency of linear resonator reaches the maximum at natural resonant frequency, while the transfer power reaches the

The associate editor coordinating the review of this manuscript and approving it for publication was Lei Zhao.

This work is licensed under a Creative Commons Attribution 4.0 License. For more information, see https://creativecommons.org/licenses/by/4.0/

maxima at the two splitting frequencies [8], [9]. Therefore, it is essential to ensure the stability of output voltage in the case of high efficiency operation. However, the transmission efficiency depends on high quality factors Q, the higher Q values mean the narrower bandwidth of the resonator. Although the linear resonator can achieve high efficiency operation at natural resonant frequency, their narrow bandwidth reduces the tolerance of the system to frequency detuning, which usually triggered by the variation of the coupling factor, variation of the load, environmental effects, component aging, allowable error or coupling to nearby objects [10].

As mentioned before, the MCR-WPT system employing traditional linear resonators is vulnerable to frequency misalignment and working frequency drift. Several methods have been reported to enhance the stability of output voltage in the case of high efficiency operation such as frequency tracking [7], [11], load impedance matching [12], [13], resonator impedance matching [14], [15] and coupling manipulation [16], [17]. It has been shown that the resonance can be maintained with the above theories. However, the frequency tracking range is restricted by regulations of the frequency management organization, impedance matching arrays only adjust the reactance in discrete values. The reported methods require sensor circuits, additional power supply, control circuit, another components (capacitor, inductor or coil), which may lead to complexity of the system, increase cost and size of the system, and increase power consumption of the system [6]. It is worth mentioning that some papers provide new methods and ideas that have inspired the authors, several examples are as follows. A variable capacitor is proposed to track power frequency by changing the natural resonant frequency, where the equivalent capacitance can be varied continuously by adjusting the DC bias of the non-linear capacitor [18]. A variable inductor is proposed to track power frequency by changing the natural resonant frequency, which use the characteristic of magnetic saturation and its equivalent inductance can be varied continuously by changing the DC bias [19]. Both of the above methods can change the reactance of the nonlinear capacitor or inductor in continuous values, the system can be operated in resonance state by adjusting the natural resonance frequency. But it is not fundamentally different from the traditional linear resonator, the problems such as complexity, cost, size, and the additional power consumption of the system still exist. The Duffing resonator (one of the nonlinear resonators) which is implemented with nonlinear capacitor is adopted in Ref. [20], [21], it has been shown that the Duffing resonator improves the bandwidth compared with the linear resonator which have similar quality factor (Q). The WPT system with parity-time (PT) symmetric Duffing resonators is presented in Ref. [22], which is implemented with nonlinear capacitor and negative resistor, it has been shown that the two issues of resonance and distance sensitivity for WPT systems can be addressed in a certain range. Although the current methods present the principle, analysis and design of the Duffing resonator for WPT system, the nonlinear resonator is composed of nonlinear capacitor and linear inductor, it is difficult to find or construct nonlinear capacitor which is suitable for low-frequency and high-power applications [23]. Therefore, it is necessary to research low-frequency and high-power Duffing resonator employing nonlinear inductor and linear capacitor for WPT system.

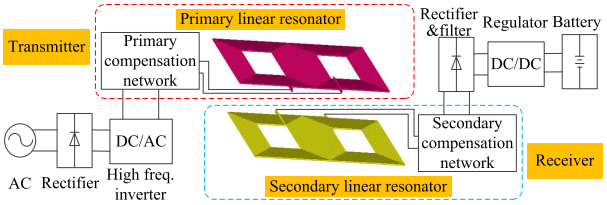

FIGURE 1. The typical block diagram of the MCR-WPT system.

As shown in Fig. 1, different primary and secondary compensation networks constitute MCR-WPT systems with different topologies, and different topologies show different output characteristics. By adding parallel saturation inductor to MCR-WPT system with different topologies, the NLR-WPT system with corresponding topologies can be constructed. This method is suitable for MCR-WPT system in various topologies such as SS (series-series), SP (series-parallel), PS (parallel-series), PP (parallel-parallel) or high-order compensation network. Therefore, on the basis of the traditional MCR-WPT system, a variety of NLR-WPT system with novel and different topologies can be implemented. The proposed NLR-WPT system can automatically track the power frequency by adjusting the natural resonance frequency without the need to modulate the source frequency, add additional active control circuits, or utilize impedance matching networks. The non-linear resonator can be usually described by a set of second-order differential equations with cubic nonlinearity, collectively referred to as Duffing resonator. The NLR-WPT system can maintain a similar output voltage value over wide bandwidth compared with the traditional WPT system, and its bandwidth is independent of the quality factor (Q). The presented method can effectively enhance tolerance to frequency misalignment and frequency drift of the WPT system. Furthermore, the NLR-WPT system can also effectively improve the position-insensitive capability by employing a nonlinear resonator at the receiver side.

This paper is organized as follows. The background and characteristics of the Duffing resonator are discussed in Section II. The principle, analysis and circuit design of nonlinear resonator using magnetic saturation inductor are described in Section III. The experiment and result analysis are presented in Section IV.

II. THE BACKGROUNG AND CHARACTERISTICS OF THE DUFFING RESONATOR

Duffing nonlinearity, named after Georg Duffing, is one of the most widely explored nonlinear vibratory phenomena in the engineering field. The oscillatory system relevant to such nonlinear dynamics is called the Duffing resonator and the differential equation which is used to characterize the dynamics is called the Duffing equation [24], [25].

The Duffing equation is a second-order differential equation with cubic nonlinear term, the original purpose was to describe mechanical vibration in terms of nonlinear restoring forces [23], [26]. If the viscous damping is not neglected, the Duffing equation can be obtained as

$$\ddot{x} + \beta\dot{x} + \omega_0^2 x + \alpha x^3 = F\cos\omega t, \tag{1}$$

where x is displacement, β is the coefficient of damping term, ω_0 is the natural vibration frequency, α is the coefficient of the third-order nonlinear term, and $F\cos\omega t$ is the excitation, where F represents amplitude, $\omega = 2\pi f$ represents power angular frequency, and f represents power supply frequency.

The approximate steady-state solution of (1) can be expressed as

$$x(\omega, t) = A(\omega)\cos(\omega t - \theta), \tag{2}$$

where "A" represents the resonance amplitude which is relevant to angle frequency ω, and θ represents the phase difference in relation to the power supply [27], [28]. The response amplitude "A" as a function of power supply frequency can be gotten from

$$A^2[(\omega_0^2 - \omega^2) + 0.75\alpha A^2]^2 + (\beta A\omega)^2 = F^2. \tag{3}$$

The typical frequency-amplitude response curve of a Duffing resonator is shown in Fig. 2(a). It is different from the central symmetric bell-shaped response curve of a linear resonator, the frequency-amplitude response peak of the Duffing resonator is "tilted" to the right side, also known as hysteretic characteristic. Due to the hysteretic characteristic of the Duffing resonator, making for a particular frequency range where three distinct response values are existed (referred to as the particular frequency range). However, the middle solution points are unstable, the steady-state response of Duffing resonator converges to the upper equilibrium points or the lower equilibrium points according to the preliminary conditions [29], [30]. If the input excitation amplitude is constant, the resonance amplitude changes along the point 1, 2, 3, 4, 5 when the power frequency f increases tardily, and the amplitude jumps from point 3 to point 4 (the point 3 is known as the jump-down point). Similarly, the amplitude varies along points 5, 4, 6, 7, 2, 1 when the excitation frequency f decreases slowly, and the amplitude jumps from point 6 to point 7 (the point 6 is known as the jump-up point). The amplitude of the resonator described by the Duffing equation suddenly increases or decreases depending on the boundary frequency of the jumping point, such behavior is called a jumping phenomenon [31].

As can be seen from Fig. 2(b), The frequency-amplitude response characteristic is dependent on α (the coefficient of third-order nonlinear term). The response curve is symmetric bell-shaped when $\alpha = 0$, the response curve is bending to the right side (called hardening systems) when $\alpha > 0$, and the response curve is bending to the left side (called softening systems) when $\alpha < 0$ [32]. The peak response of the nonlinear resonator is bending to the left or right side,which increase

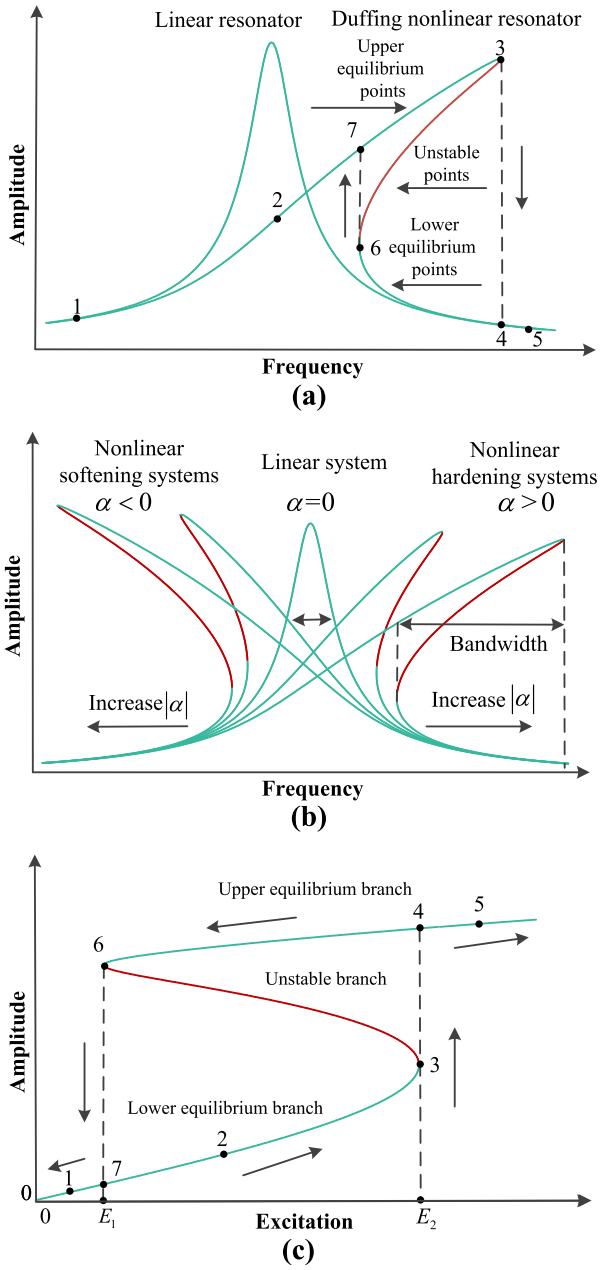

FIGURE 2. The features curves of the Duffing resonator: (a) Amplitude versus frequency response ; (b) Amplitude versus frequency response with different α; (c) Response amplitude versus excitation amplitude.

the bandwidth compared to the linear resonator having the similar quality factor Q. Therefore, a properly designed Duffing resonator can achieve a much wider bandwidth by adjusting the value of α. The purpose of using Duffing resonator in WPT is to tap into the bending characteristic of the response as a means of solving the amplitude-bandwidth limitation issue.

The curve of the response amplitude as a function of the excitation amplitude is shown in Fig. 2(c). It can be seen that the steady-state response of Duffing resonator converges to the upper or the lower equilibrium branch based on the preliminary conditions. If the system operates at the desired

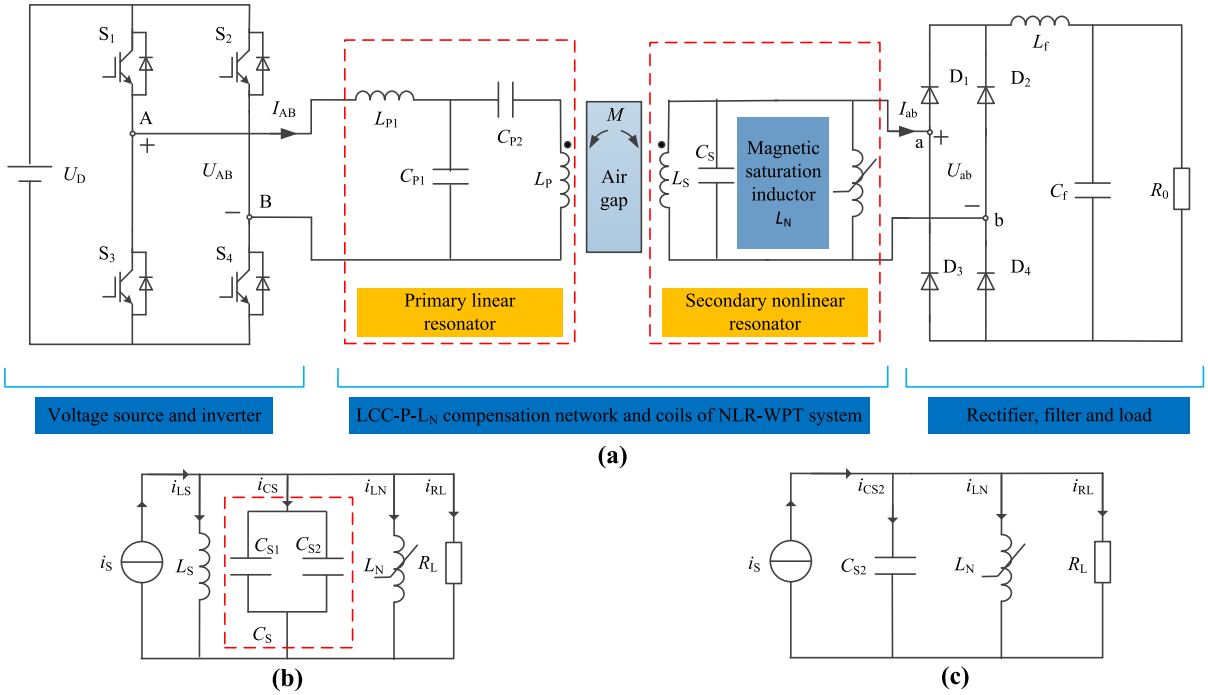

FIGURE 3. The basic schematic circuit of the NLR-WPT system and its equivalent circuits: (a) The basic schematic circuit of the NLR-WPT system; (b) The equivalent circuit of the NLR-WPT system; (c) The simplified equivalent circuit of the NLR-WPT system.

source frequency, the resonance amplitude changes along the point 1, 2, 3, 4, 5 when the excitation amplitude increases slowly, and the amplitude jumps from point 3 to point 4. Similarly, the amplitude varies along points 5, 4, 6, 7, 1 when the excitation amplitude decreases tardily, and the amplitude jumps from point 6 to point 7. Due to the hysteretic characteristic, the response amplitude remains constant basically regardless of the variation of the excitation amplitude in a certain range. Therefore, the output response amplitude of NLR-WPT system can be maintained as the coupling coefficient varies.

III. PRINCIPLE, ANALYSIS, AND DESIGN OF NONLINEAR RESONATOR FOR NLR-WPT SYSTEM

In this paper, a NLR-WPT system with LCC-P-L_N topology is implemented by adding parallel saturated inductor based on the traditional linear LCC-P topology WPT system. The basic schematic circuit of the NLR-WPT system described in this paper is shown in Fig. 3(a). The primary resonator is linear, while the secondary resonator is nonlinear due to the introduction of magnetic saturation inductor. For the purpose of studying the overall circuit characteristics, an equivalent resonant circuit with the same behavior can be developed by decoupling the primary coil and secondary coil, as shown in Fig. 3(b). The secondary compensation capacitance C_S can be splitted into two parts – C_{S1} and C_{S2}, and the correlation among them can be expressed as $C_S = C_{S1} + C_{S2}$. If the nonlinear system can be replaced with an equivalent linearized system, the NLR-WPT system can be further simplified as Fig. 3(c) when parallel resonance occurs between the secondary inductance L_S and a part of secondary capacitance C_S, i.e., C_{S1}.

The equivalent parallel nonlinear resonator consists of a sinusoidal equivalent excitation current source i_S, compensation capacitance C_{S2}, equivalent "average" inductance L_N and equivalent load R_L. The equivalent excitation current source $i_S = I_S\cos(\omega t) = \sqrt{2}\frac{\omega M I_P}{L_S}\cos(\omega t)$, where I_P is current RMS value of primary coil, $\omega = 2\pi f$ is angular frequency, M is the mutual inductance between the primary coil and the secondary coil, L_S is inductance of secondary coil (according to the characteristics of LCC-P compensation network). The equivalent capacitance C_{S2} is a part of C_S which resonate with nonlinear inductor. As shown in Fig. 6, the L_N and i_{LN} relationship of the nonlinear inductor is symmetric (even function of current), i.e., $L_N(i_{LN}) = L_N(-i_{LN})$, where i_{LN} is the current through the nonlinear inductor. Ignoring the inherent loss of the resonator, the equivalent load R_L which include the diode rectifier, filter and resistive load R_0 can be calculated by $R_L = \frac{\pi^2}{8}R_0$.

The time-domain dynamic equation representing the properties of the nonlinear parallel RLC resonant circuit can be procured by applying the Kirchhoff current law (KCL) and with the use of $u = d\psi/dt$

$$i_{LN} + \frac{1}{R_L}\frac{d\psi_{LN}}{dt} + C_{S2}\frac{d^2\psi_{LN}}{dt^2} = i_S, \tag{4}$$

where $i_S = I_S\cos(\omega t)$ is sinusoidal excitation current, i_{LN} is the current across the nonlinear inductor, and $\psi_{LN}(t)$ is the amount of magnetic flux stored in the nonlinear inductor. In order to describe the current across the nonlinear inductor

on the basis of ψ_{LN}, the detailed analysis is applied as follows

$$d\psi_{LN} = L_N di_{LN} + i_{LN} dL_N. \tag{5}$$

Thus, the total amount of stored magnetic flux during one period can be calculated by

$$\begin{aligned}\psi_{LN} &= \int (L_N di_{LN} + i_{LN} dL_N) \\ &= \int (L_N + i_{LN}\frac{dL_N}{di_{LN}}) di_{LN}.\end{aligned} \tag{6}$$

Because of the L_N and i_{LN} symmetric correlation of nonlinear inductor, the L_N and i_{LN} relationship is approximately described by a Taylor polynomial of order n, where the odd-order terms in the Taylor expansion of (7) vanishes and the even-order terms can be used to express the weak nonlinearity of L_N

$$L_N = L_0 + L_2 i_{LN}^2 + L_4 i_{LN}^4 + L_6 i_{LN}^6 + \cdots + L_n i_{LN}^n. \tag{7}$$

By substituting (7) into (6), ψ_{LN} can be described as

$$\psi_{LN} = \int \sum_{i=0}^{n(even)} (i+1) L_i i_{LN}^i di_{LN} = \sum_{i=0}^{n(even)} L_i i_{LN}^{i+1}. \tag{8}$$

Therefore, i_{LN} can be expressed in terms of ψ_{LN} according to inverse Taylor expansion. In order to express nonlinear resonator in the form of Duffing equation, neglecting the higher than third-order terms for simplicity, i_{LN} can be written as

$$i_{LN} = \frac{1}{a_1}\psi_{LN} + \frac{1}{a_3}\psi_{LN}^3, \tag{9}$$

where $a_1 = L_0$ is the inverse of the linear coefficient, and a_3 is the inverse of the nonlinear coefficient. In general, a_1 and a_3 can be approximately obtained from the inductor-current relationship for any nonlinear inductor. Substituting (9) into (4) results in

$$\begin{aligned}\frac{d\psi_{LN}^2}{dt} + \frac{1}{R_L C_{S2}}\frac{d\psi_{LN}}{dt} + \frac{1}{a_1 C_{S2}}\psi_{LN} \\ + \frac{1}{a_3 C_{S2}}\psi_{LN}^3 = \frac{I_S}{C_{S2}}\cos(\omega t).\end{aligned} \tag{10}$$

It's worth noting that (10) has the same form as the Duffing equation presented in (1). The solution of (10) can also be described as a sinusoidal function $\psi_{LN}(t) = \psi_m \cos(\omega t - \theta)$, where ψ_m is the response amplitude of time dependent magnetic flux, i.e., the maximum amount of magnetic flux stored in the inductor during one cycle, and θ represents the phase difference in respect of the power supply.

The restoring force consist of both the linear term $\frac{1}{a_1 C_{S2}}\psi_{LN}$ and the third-order nonlinear term $\frac{1}{a_3 C_{S2}}\psi_{LN}^3$. In order to facilitate the analysis, an equivalent linear inductance L_{eff} can be defined to quantify the restoring force which is contributed by the nonlinear term, according to the law of conservation of energy, the following relation can be obtained

$$\begin{aligned}\int_0^{\frac{T}{4}} \frac{d(\frac{1}{L_{eff}C_{S2}}\psi_{LN})}{dt}\frac{\frac{1}{L_{eff}C_{S2}}\psi_{LN}}{L_N} dt \\ = \int_0^{\frac{T}{4}} \frac{d(\frac{1}{a_3 C_{S2}}\psi_{LN}^3)}{dt}\frac{\frac{1}{a_3 C_{S2}}\psi_{LN}^3}{L_{eff}} dt.\end{aligned} \tag{11}$$

According to (11), L_{eff} can be calculated as

$$L_{eff} = \frac{a_3}{\psi_m^2}. \tag{12}$$

In the actual system, the nonlinear term only exists in part of each cycle, so L_{eff} should be multiplied by a coefficient greater than 1, but the coefficient does not affect the system analysis qualitatively. Because the nonlinear term is linearized, (9) can be written as

$$i_{LN} = \frac{1}{a_1}\psi_{LN} + \frac{1}{a_3}\psi_{LN}^3 = \frac{1}{L_0}\psi_{LN} + \frac{1}{L_{eff}}\psi_{LN}, \tag{13}$$

Hence, equivalent "average" inductance L_N can be expressed as

$$\frac{1}{L_N} = \frac{1}{L_0} + \frac{1}{L_{eff}}, \tag{14}$$

based on (12), (13) and (14), the natural frequency of the Duffing resonator ω_0 can be derived as

$$\omega_0 = \sqrt{\frac{1}{C_{S2}}\frac{1}{L_N}} = \sqrt{\frac{1}{C_{S2}}(\frac{1}{a_1} + \frac{\psi_m^2}{a_3})}. \tag{15}$$

Similarly, equation (10) can be written as

$$\begin{aligned}\frac{d\psi_{LN}^2}{dt} + \frac{1}{R_L C_{S2}}\frac{d\psi_{LN}}{dt} + \frac{1}{a_1 C_{S2}}\psi_{LN} \\ + \frac{1}{L_{eff}C_{S2}}\psi_{LN} = \frac{I_S}{C_{S2}}\cos(\omega t).\end{aligned} \tag{16}$$

Furthermore, differential equations (16) can be written in frequency domain form, the amplitude-frequency relationship of the circuit is given by

$$(j\omega)^2 Z + \frac{1}{R_L C_{S2}}(j\omega)Z + (\frac{1}{a_1 C_{S2}} + \frac{1}{L_{eff}C_{S2}})Z = \frac{I_S}{C_{S2}}, \tag{17}$$

where, $Z = \psi_m e^{-j\theta}$ is the phasor form of $\psi_{LN}(t)$. Finally, substituting (12) in (17) results in

$$\psi_m^2(\omega_0^2 - \omega^2)^2 + (\frac{1}{R_L C_{S2}}\psi_m\omega)^2 = (\frac{I_S}{C_{S2}})^2. \tag{18}$$

The magnetic flux amplitude ψ_m can be obtained from (18) as a function of ω, Subsequently, the magnetic flux can be calculated using equation $\psi_{LN}(t) = \psi_m \cos(\omega t - \theta)$ and current i_{LN} can be calculated from (9).

Based on the above analysis, the following conclusions can also be drawn:

1) The saturation inductor with L_N and i_{LN} symmetric correlation curve has $a_3 > 0$, the NLR-WPT system containing such magnetic saturation inductor have a frequency response bending to the right;

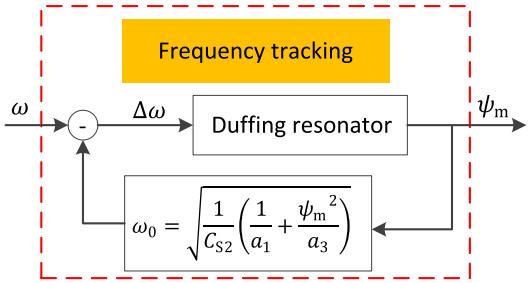

FIGURE 4. Negative feedback of the NLR-WPT system, showing the feedback term provided by the magnetic saturation inductor.

2) The equivalent linear inductance L_{eff} is closely related to the resonance amplitude during one resonant cycle. More specifically, the higher the response amplitude, the smaller the equivalent inductance, vice versa;
3) The nature resonance angular frequency ω_0 of the NLR-WPT system can automatically track excitation angular frequency ω by adjusting its own inductance value. Assuming that the NLR-WPT system originally converges to the upper equilibrium points, when the excitation frequency ω is reduced, the amplitude of magnetic flux will decrease, so the equivalent "average" inductance will increase. The increase of inductance value will result in decrease of the natural resonance frequency, vice versa;
4) As shown in Fig. 4, the nonlinear resonator has the function of negative feedback due to the introduction of magnetic saturation inductor, which decrease the difference value between the excitation angular frequency ω and the natural resonance angular frequency ω_0. Therefore, The NLR-WPT system described in this paper can effectively enhance the tolerance to frequency misalignment and frequency drift, and the amplitude-bandwidth limitation issue can also be solved.

The L_{N} and i_{LN} relationship of the nonlinear inductor can be provided by a plurality of coils wound around a magnetic ring. As shown in Fig. 5, the magnetic ring is made of TDK PC95 material, its outside diameter, inner diameter and height are 25mm, 15mm, and 13mm, respectively. According to electromagnetic equation $\text{B} = \mu\text{H}$ and $\text{Hl} = \text{NI}$, the characteristic curve of PC95 magnetic ring can be measured and calculated. It can be seen that the relative permeability μ_{r} of magnetic ring varies as magnetic field intensity H varies. Therefore, the value of the saturated inductance L_{N} will change with the variation of the current i_{LN}.

Based on the magnetic saturation characteristic of the magnetic ring, the magnetic saturation inductor is designed by the following equation

$$L_{\text{N}} = N^2 \frac{\mu_0 \mu_{\text{r}} S}{l}, \tag{19}$$

where N is the coil turns wound around the magnetic ring, S is cross-sectional area of magnetic ring, l is circumference of magnetic ring, $\mu_0 = 4\pi 10^{-7} N\text{A}^{-2}$ is vacuum permeability, μ_{r} is relative permeability.

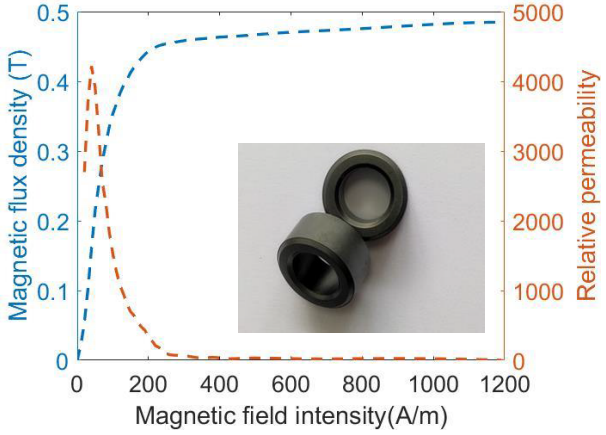

FIGURE 5. The characteristic curve of PC95 magnetic ring. Insert figure: Photo of TDK PC95 magnetic ring.

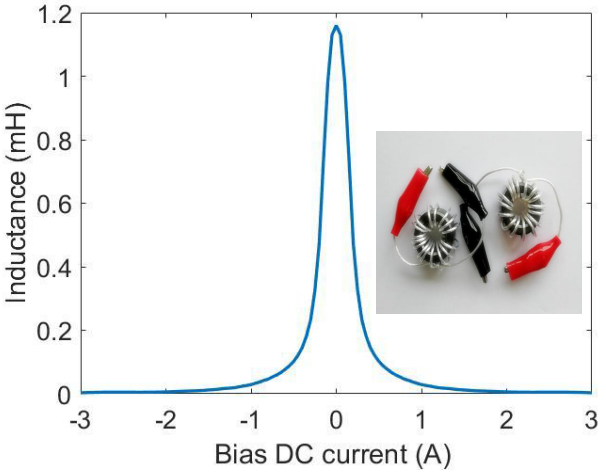

FIGURE 6. The L_{N} and i_{LN} relation curve of the magnetic saturation inductor. Insert figure: Photograph of the magnetic saturation inductor designed in this paper.

Furthermore, the equation that describes the output voltage and the magnetic flux of the saturation inductor is given by

$$U_0 = 4.44 f N \psi_{\text{m}}, \tag{20}$$

where U_0 is output voltage of the saturation inductor, f is frequency, $\psi_{\text{m}} = \text{BS}$ is saturation magnetic flux.

Based on the above analysis, an experimental saturation inductor containing 16 turns coils have been designed. As shown in Fig. 6, the L_{N} is even function of current, i.e., $L_{\text{N}}(i_{\text{LN}}) = L_{\text{N}}(-i_{\text{LN}})$. It is worth noting that the appropriate operating frequency of the NLR-WPT system is mainly determined by the magnetic core material. If the operating frequency exceeds this frequency, the eddy current loss will increase rapidly and the magnetic core temperature will also increase. With the development of magnetic core material, the magnetic core suitable for all kinds of standard frequency of WPT system can be within reach. Therefore, the saturation inductor can be designed over different frequency ranges by selecting different magnetic ring (including materials and dimensions). According to (19) and (20), the output voltage

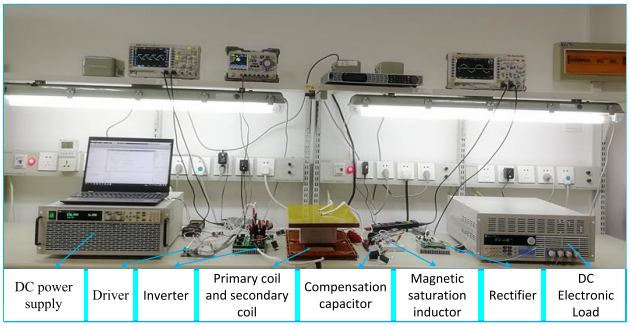

FIGURE 7. The Photograph of the NLR-WPT system prototype.

and power of the NLR-WPT system can be adjusted by changing the number of turns or wire running method wound around the magnetic ring.

IV. THE EXPERIMENT AND RESULT ANALYSIS

In order to verify the analysis of the proposed NLR-WPT system with nonlinear resonator, an experimental prototype using the configuration of Fig. 3(a) has been built. The prototype has been designed to operate at approximately 30 kHz with a similar output voltage of 140 V and a maximum power of 300 W. It is constructed by adding parallel saturated inductor at the receiving end of the traditional linear LCC-P topology WPT system, and the saturated inductor is the key to the efficient and stable operation of the system. Therefore, it is necessary to adopt appropriate materials and sizes of magnetic rings, and design the corresponding nonlinear inductor according to the standard of frequency range, power level, distance, etc., so as to study the standardized and practical NLR-WPT system.

The photograph of the NLR-WPT prototype is shown in Fig. 7, the experiment system consist of ITECH auto range power supply, driver, full-bridge inverter, primary linear resonator, secondary nonlinear resonator, rectifier, MAYNUO DC electronic load, RIGOL oscilloscope, etc. Here, four drivers used to drive inverter switchs are 1EDI20N12AF, the inverter MOSFETs are C3M0120090 and rectifier diodes are IDW20G65C5SiC. The output filter uses L_f of 60 μH and C_f of 6 μF. The parameters of primary resonator and secondary resonator are measured and listed in Table 1. Both the primary coil and secondary coil adopt DD structure, i.e., double D coil, where DD type coil is composed of two rectangular coils connected in parallel and magnetic circuits in series. As shown in Fig. 1, the upper coil is the DD type transmitting coil and the lower coil is the DD type receiving coil, and their self-inductance satisfy $L_{\mathrm{P}} = L_{\mathrm{S}} = 112\,\mu$H. The primary compensation network consist of $L_{\mathrm{P1}} = 56\,\mu$H, $C_{\mathrm{P1}} = 0.47\,\mu$F, and $C_{\mathrm{P2}} = 0.47\,\mu$F (parameters can be obtained from the principle of linear LCC compensation $\omega = 1/\sqrt{LC}$). The capacitance of secondary compensation network $C_{\mathrm{S}} = 0.34\,\mu$F, where C_{S} is splitted into two parts – C_{S1} and C_{S2}, the correlation among them can be expressed as $C_{\mathrm{S}} = C_{\mathrm{S1}} + C_{\mathrm{S2}}$. C_{S1} can be obtained from the principle of linear compensation $\omega = 1/\sqrt{L_{\mathrm{S}}C_{\mathrm{S1}}}$, as a rule of thumb, C_{S2} is generally 0.5 times of C_{S1}.

TABLE 1. Parameters of the experimental prototype.

Symbol	Note	Values
L_{P}	Self-inductance of primary-side coil	112 μH
L_S	Self-inductance of secondary-side coil	112 μH
L_{P1}	Inductance of primary compensation network	56 μH
C_{P1}	Shunt capacitance of primary compensation network	0.47 μF
C_{P2}	Series capacitance of primary Compensation network	0.47 μF
C_{S}	Capacitance of secondary Compensation network	0.34 μF
f	Optimum operating frequency in linear state	$\sim$ 31 kHz
k	Coupling coefficient	0.27

A. WAVEFORMS ANALYSIS OF NLR-WPT SYSTEM IN LINEAR AND NONLINEAR STATE

The experimental waveforms of NLR-WPT system in linear state are shown in Fig. 8 (a)-(b) when $f = 30.9$ kHz, $I_{\mathrm{P}} = 6$ A, $R_0 = 100\,\Omega$, and $C_{\mathrm{S}} = 0.34\,\mu$F. It can be seen that output voltage and current of linear state are standard sine wave, zero voltage switching (ZVS) can be realized through a weak inductive input impedance. The reason for such behaviors is that the current across the nonlinear inductor is too small and the inductor is not saturated. The inductance value of saturated inductor is very large compared with that of the secondary side coil, so the saturation inductor branch is almost equivalent to open circuit. All else being equal, when $I_{\mathrm{P}} = 10$ A, the system goes into a nonlinear state due to the inductor is saturated. As shown in Fig. 8 (c)-(d), ZVS can also be realized, the waves of output voltage and current are quite different compared with that of the traditional linear state. As the current increases, the nonlinear inductor goes into saturated condition, the value of the nonlinear inductor becomes small, and the inductance value is closely related to the response amplitude. The current flowing through the saturation inductor changes dramatically, and the voltage waveform is no longer a sine wave.

The NLR-WPT system requires certain excitation conditions to transfer the secondary resonator from linear working state to nonlinear resonant state. It can be operated in nonlinear resonate state by increasing the amplitude of the excitation or adjusting the power frequency to the optimum operating frequency. Furthermore, the experiment results show that as long as the NLR-WPT system enters nonlinear resonant state, the output voltage waveform is stable and the RMS value of output voltage is basically unchanged, even while the power frequency, excitation amplitude, equivalent load, compensation capacitance and coupling coefficient vary in a certain range (the experiments and detailed analysis are described below). Therefore, the NLR-WPT system described in this paper has high robustness.

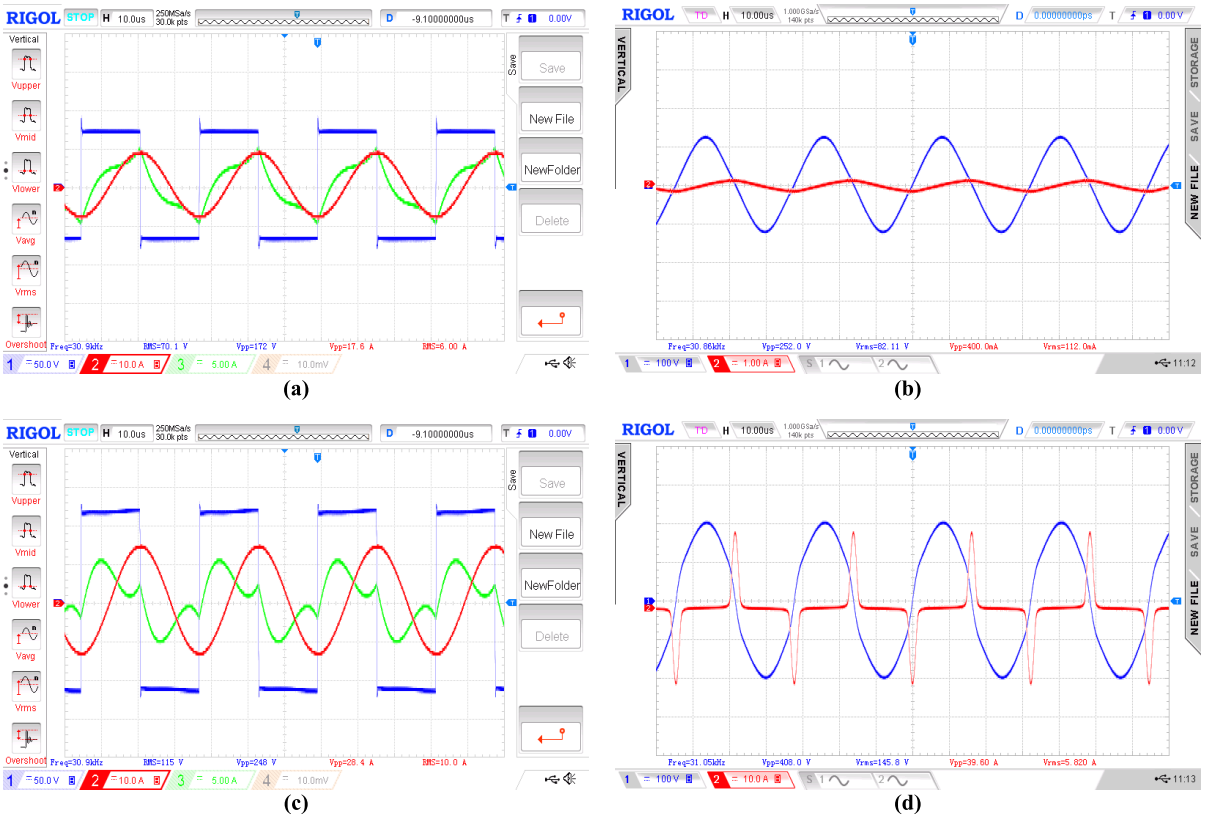

FIGURE 8. Experimental waveforms of NLR-WPT system in the linear and the nonlinear states:(a) Input voltage, current and primary coil current waveforms of linear state; (b) Output voltage and current waveforms of magnetic saturation inductor in linear state;(c) Input voltage, current and primary coil current waveforms of nonlinear state;(d) Output voltage and current waveforms of magnetic saturation inductor in nonlinear state.

B. HYSTERESIS AND JUMPING CHARACTERISTICS OF THE NLR-WPT SYSTEM

The frequency response of the NLR-WPT system is measured to study its hysteresis and jumping characteristics. According to the characteristics of LCC-P compensation topology, the equivalent excitation current source of the secondary nonlinear resonator $i_S = \sqrt{2}\frac{\omega M I_P}{L_S}\cos(\omega t)$. The voltage-frequency waveforms are shown in Fig. 9 where the operation frequency is varied continuously from 25.6 kHz to 36.5 kHz. It can be seen that the output voltage changes along the upper curve (nonlinear resonant state curve) when the excitation frequency f increases tardily, and the output voltage jumps from point 1(35.1 kHz corresponds to the jump-down point) to point 2. Similarly, the output voltage varies along the bottom curve (linear resonant state curve) when the excitation frequency f decreases slowly, and the output voltage will jump from point 3 (32.5 kHz corresponds to the jump-up point) to point 4. Therefore, the experimental results show that the NLR-WPT system has hysteresis and jumping characteristics, which also proves the correctness of simplifying the model based on Duffing equation.

C. BANDWIDTH ENHANCEMENT

The frequency response of the NLR-WPT system is measured to study its bandwidth enhancement capability. Fig. 10 shows

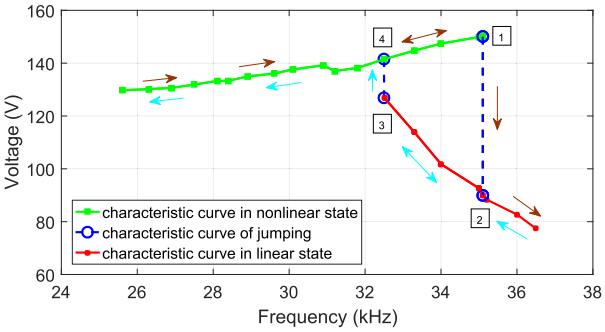

FIGURE 9. The hysteresis and jumping characteristics curve of the NLR-WPT system with $I_P = 10$ A, $R_0 = 100\,\Omega$, and $C_S = 0.34\,\mu$F.

the output voltage-frequency (ranging from 25.6 kHz to 36.5 kHz) waveforms at three different current RMS value of primary coil $I_P = 6$ A, 8.5 A, and 10 A, respectively. It can be seen that when $I_P = 6$ A, the system enters a linear state due to the inductor is not saturated. When $I_P = 8.5$ A or 10 A, the system goes into a nonlinear state due to the inductor is saturated. The bandwidth in this paper is defined as the frequency range where the output voltage amplitude is greater than $1/\sqrt{2}$ of its maximum value. It should be noted that the bandwidth in the nonlinear state(25.6 kHz-35 kHz) is 1.7 times larger than that in the

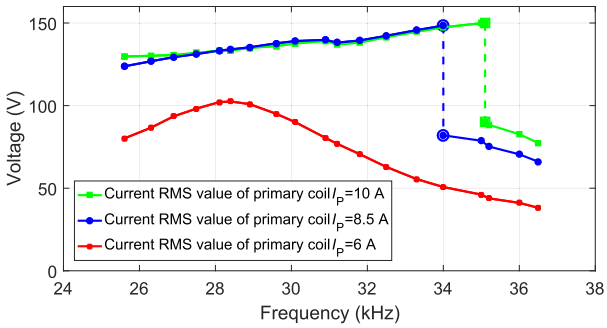

FIGURE 10. Comparison of the measured output voltage versus frequency in the linear state and the nonlinear state with $R_0 = 100\,\Omega$, and $C_S = 0.34\,\mu$F.

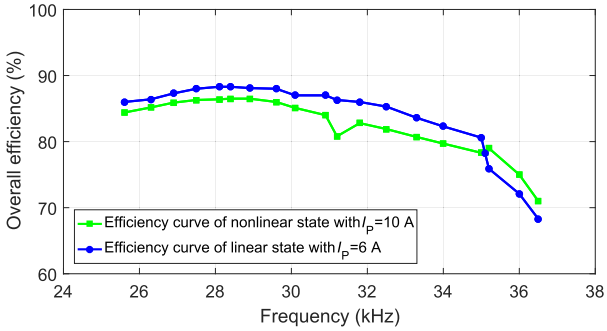

FIGURE 11. Comparison of the measured power transfer efficiency versus frequency between the nonlinear state and the linear state with $R_0 = 100\,\Omega$, and $C_S = 0.34\,\mu$F.

linear state (25.6 kHz-31.2 kHz). When $I_P = 10$ A (denoted by green color curve), the output voltage stabilizes at the same level, and the fluctuation between the maximum voltage and minimum voltage is less than 12.46% over the power frequency ranging from 25.6 kHz to 35.1 kHz. When the operation frequency is varied continuously from 25.6 kHz to 31.8 kHz, the output voltage fluctuation is only less than 5%. Therefore, the NLR-WPT system employing the nonlinear resonator at the receiver side can effectively enhance tolerance to frequency misalignment and frequency drift. In addition, such NLR-WPT system can maintain a similar output voltage value over wide bandwidths compared with traditional WPT system.

The influence of the available power level (current RMS value of primary coil) on the performance of NLR-WPT system has been studied, as showed in Fig. 10. It can be seen that the system goes into nonlinear state when $I_P = 8.5$ A or 10 A. The slopes of the output voltage-frequency curves are not affected by the current RMS value of primary coil. It can be also seen that with the increase of the current RMS value, the peak of output voltage increases, and the jump-down point transfers to higher frequencies. The reason for such a characteristic is that the equivalent average inductance of the magnetic saturation inductor decreases with the increase of current swing across it.

The power transfer efficiency η of the NLR-WPT system as a function of excitation frequency is shown in Fig. 11. The overall efficiency η is calculated by P_{out}/P_{in}, where P_{in} is the system input power of DC power supply, P_{out} is the system output power of DC electronic load. When $I_P = 10$ A, the NLR-WPT system goes into a nonlinear state, high efficiency over 78.3% is maintained in the range of f from 25.6 kHz to 35.1 kHz. When the operation frequency is varied continuously from 25.6 kHz to 31.2 kHz, the system overall efficiency is not less than 84%, and high overall efficiency of 86.5% can be achieved under a wide range of frequency (27.5 kHz-30.1 kHz). The overall efficiency in the nonlinear state is slightly less than that in the linear state under the same frequency. The reason for such phenomenon is that the heating of magnetic saturation inductor increases the losses of the NLR-WPT system. When the NLR-WPT system enters the linear state, the saturated inductor branch is almost equal to open circuit, and the nonlinear inductor has no loss. When the NLR-WPT system enters the nonlinear resonant state, the nonlinear inductor participates in the resonance, the temperature of the nonlinear inductor increases, and the system generates additional losses. The nonlinear inductor losses is composed of copper loss and iron loss, the copper loss of the coil can be ignored, and the iron core loss is closely related to the magnetic material characteristics, working frequency and temperature. Although the efficiency of linear system is slightly higher, the stability of output voltage is far behind that of the nonlinear system designed in this paper. In actual application, the traditional linear WPT system often needs an extra DC-DC voltage regulating module at the output end due to large voltage fluctuation, which increases the loss of the system. The NLR-WPT system can be designed without voltage regulation module, so the efficiency of the practical MCR-WPT system and the NLR-WPT system is very close.

D. THE INFLUENCES OF PARAMETERS VARIATION ON THE NLR-WPT SYSTEM

The effect of the secondary compensation capacitance values on the performance of NLR-WPT system has been investigated experimentally. When the working frequency is varied continuously from 25.6 kHz to 36.5 kHz, Fig. 12 shows the output voltage-frequency waveforms at three different compensation capacitance $C_S = 0.3\,\mu$F, 0.34 μF, and 0.38 μF, respectively. When $C_S = 0.3\,\mu$F, the frequency of jump-down point is 35.1 kHz, and the peak output voltage is 153.1 V. When $C_S = 0.38\,\mu$F, the frequency of jump-down point is 35 kHz, and the peak output voltage drops to 146.5 V. The voltage-frequency curves for different compensation capacitance values have similar slopes. It can be also observed that the output voltage fluctuation varies significantly when the NLR-WPT system changes from the nonlinear resonant state to the linear resonant state, which also proves that the sensitivity of nonlinear resonance WPT system to parameters is lower than that of linear resonance WPT systems.

The influence of different load values on the operation of the NLR-WPT system has been studied experimentally. Fig. 13 shows the waveforms at three different load

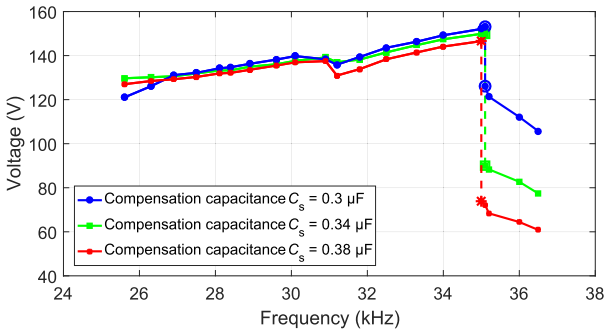

FIGURE 12. Experimental results when $I_P = 10$ A and $R_0 = 100\,\Omega$ under three different compensation capacitors C_S.

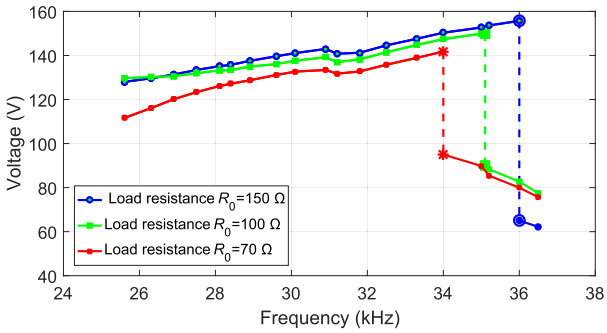

FIGURE 13. Comparison of the measured output voltage versus frequency when $I_P = 10$ A and $C_S = 0.34\mu$F under different load R_0.

resistances $R_0 = 70\,\Omega$, $100\,\Omega$, and $150\,\Omega$, respectively. It can be observed that as the load resistance increases, the peak of output voltage increases, and the jump-down point transfers to higher frequencies. When $R_0 = 150\,\Omega$, the frequency of jump-down point is 36 kHz, and the peak output voltage is 155.7 V. When $R_0 = 70\,\Omega$, the frequency of jump-down point drops to 34 kHz, and the peak output voltage drops to 141.7 V. Moreover, the slopes of the voltage-frequency curves are not affected by the variation of load resistance. Therefore, the bandwidth of the NLR-WPT with magnetic saturation inductor is not obviously influenced by load resistance. This characteristic is obviously different from the response of a traditional MCR-WPT system whose bandwidth is proportional to load resistance value.

In order to improve the anti-offset ability of the system, both the primary coil and secondary coil adopt DD structure. When the vertical distance between transmitting and receiving coils is 10 cm and there is no deviation in the horizontal direction, the coupling coefficient $k = 0.27$. When the receiving coil is shifted 5 cm from the transmitting coil in the X-axis direction, the coupling coefficient is 0.25. when the receiving coil is shifted 5 cm from the transmitting coil in both the X-axis direction and the Y-axis direction, the coupling coefficient is 0.22. The frequency response as a function of the coupling coefficient has been investigated experimentally. Fig. 14 shows the waveforms at three different coupling coefficients $k = 0.27$, 0.25, and 0.22, respectively. It can be observed that the output

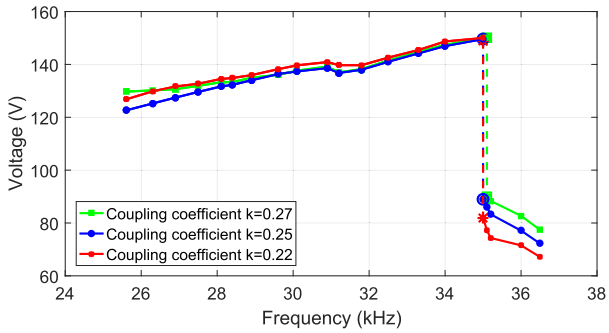

FIGURE 14. Experimental results when $I_P = 10$ A, $R_0 = 100\,\Omega$, and $C_S = 0.34\,\mu$F under different coupling coefficient k.

voltage maintains a similar resonance amplitude in the case of different coupling coefficients. As the coupling coefficient is varied, the amount of energy which is transmitted to the receiver varies correspondingly. The secondary coil can be equivalent to a variable excitation source, the excitation current source $i_S = \sqrt{2}\frac{\omega M I_P}{L_S}\cos(\omega t)$, where $M = k\sqrt{L_P L_S}$, i.e., the excitation current source i_S changes with the variation of coupling coefficient k. Due to the hysteretic characteristic of the nonlinear resonator, the response amplitude remains constant basically regardless of the variation of the equivalent excitation amplitude. Thus, the output voltage of the load is kept basically constant as the coupling coefficient varies in a certain range. The NLR-WPT system employing the nonlinear resonator at the receiver side can effectively improve the position-insensitive capability.

E. SELECTION OF OPERATION POINT

Based on the experiment and result analysis, the optimal operating point can be determined. In order to attain stable output voltage under parameters variation, the NLR-WPT system should be operated in nonlinear state by increasing the amplitude of the excitation power supply or adjusting the power frequency to the optimum operating frequency. If the input excitation amplitude is constant, the peak output voltage of NLR-WPT system appears at the jump-down frequency. If the system operates at the desired source frequency, the amplitude will increase as the excitation increase slowly. However, the jump point will move due to a wide range of changes in excitation amplitude, load and coupling coefficient. Therefore, when selecting the working point, a safety margin should be established to ensure that the working point is not too close to the jump-down frequency based on the preconditions as well as the needs.

V. CONCLUSION

This paper presents a novel NLR-WPT system with enough bandwidth and high robustness, which is implemented with a nonlinear resonator at the receiver side. Compared with conventional linear resonance WPT system, the NLR-WPT system can achieve 1.7 times bandwidth while the output voltage fluctuations is smaller and the overall efficiency can maintain the similar level. Since the magnetic saturation

inductor used for the nonlinear resonator is a passive component, the method is simple, low cost, and high efficient. The approach can automatically track the power supply frequency by adjusting the natural resonance frequency without the need to modulate the source frequency, add additional active control circuits, or utilize impedance matching networks. The NLR-WPT system designed in this paper is suitable for constant voltage charging applications, where the stable and flexible output voltage is needed over a wide frequency range under the variation of compensate capacitance, load, or coupling coefficient. In addition, the nonlinear resonator using magnetic saturation inductor can potentially be utilized for other applications such as wireless energy harvesting or impedance matching network.

REFERENCES

[1] G. A. Covic and J. T. Boys, "Inductive power transfer," *Proc. IEEE*, vol. 101, no. 6, pp. 1276–1289, Jun. 2013, doi: 10.1109/JPROC.2013.2244536.

[2] C. C. Mi, G. Buja, S. Y. Choi, and C. T. Rim, "Modern advances in wireless power transfer systems for roadway powered electric vehicles," *IEEE Trans. Ind. Electron.*, vol. 63, no. 10, pp. 6533–6545, Oct. 2016, doi: 10.1109/TIE.2016.2574993.

[3] Z. Zhang, H. Pang, A. Georgiadis, and C. Cecati, "Wireless power transfer—An overview," *IEEE Trans. Ind. Electron.*, vol. 66, no. 2, pp. 1044–1058, Feb. 2019, doi: 10.1109/TIE.2018.2835378.

[4] H. Feng, R. Tavakoli, O. C. Onar, and Z. Pantic, "Advances in high-power wireless charging systems: Overview and design considerations," *IEEE Trans. Transport. Electrific.*, vol. 6, no. 3, pp. 886–919, Sep. 2020, doi: 10.1109/TTE.2020.3012543.

[5] A. Kurs, A. Karalis, R. Moffatt, J. D. Joannopoulos, P. Fisher, and M. Soljacic, "Wireless power transfer via strongly coupled magnetic resonances," *Science*, vol. 317, no. 5834, pp. 83–86, Jul. 2007, doi: 10.1126/science.1143254.

[6] D. Shen, G. Du, W. Zeng, Z. Yang, and J. Li, "Research on optimization of compensation topology parameters for a wireless power transmission system with wide coupling coefficient fluctuation," *IEEE Access*, vol. 8, pp. 59648–59658, 2020, doi: 10.1109/ACCESS.2020.2983612.

[7] R. Huang, B. Zhang, D. Qiu, and Y. Zhang, "Frequency splitting phenomena of magnetic resonant coupling wireless power transfer," *IEEE Trans. Magn.*, vol. 50, no. 11, pp. 1–4, Nov. 2014, doi: 10.1109/TMAG.2014.2331143.

[8] Y.-L. Lyu, F.-Y. Meng, G.-H. Yang, B.-J. Che, Q. Wu, L. Sun, D. Erni, and J. L.-W. Li, "A method of using nonidentical resonant coils for frequency splitting elimination in wireless power transfer," *IEEE Trans. Power Electron.*, vol. 30, no. 11, pp. 6097–6107, Nov. 2015, doi: 10.1109/TPEL.2014.2387835.

[9] H. Zhu, B. Zhang, and L. Wu, "Output power stabilization for wireless power transfer system employing primary-side-only control," *IEEE Access*, vol. 8, pp. 63735–63747, 2020, doi: 10.1109/ACCESS.2020.2983465.

[10] W. Zhou, S. Sandeep, P. Wu, P. Yang, W. Yu, and S. Y. Huang, "A wideband strongly coupled magnetic resonance wireless power transfer system and its circuit analysis," *IEEE Microw. Wireless Compon. Lett.*, vol. 28, no. 12, pp. 1152–1154, Dec. 2018, doi: 10.1109/LMWC.2018.2876767.

[11] Y. Li, C. Zhang, Q. Yang, J. Li, Y. Zhang, X. Zhang, and M. Xue, "Improved ant colony algorithm for adaptive frequency-tracking control in WPT system," *IET Microw., Antennas Propag.*, vol. 12, no. 1, pp. 23–28, Jan. 2018, doi: 10.1049/iet-map.2017.0159.

[12] M. Fu, C. Ma, and X. Zhu, "A cascaded boost–buck converter for high-efficiency wireless power transfer systems," *IEEE Trans. Ind. Informat.*, vol. 10, no. 3, pp. 1972–1980, Aug. 2014, doi: 10.1109/TII.2013.2291682.

[13] R. Mai, Y. Liu, Y. Li, P. Yue, G. Cao, and Z. He, "An active-rectifier-based maximum efficiency tracking method using an additional measurement coil for wireless power transfer," *IEEE Trans. Power Electron.*, vol. 33, no. 1, pp. 716–728, Jan. 2018, doi: 10.1109/TPEL.2017.2665040.

[14] K. A. Cota, P. A. Gray, M. Pathmanathan, and P. W. Lehn, "An approach for selecting compensation capacitances in resonance-based EV wireless power transfer systems with switched capacitors," *IEEE Trans. Transport. Electrific.*, vol. 5, no. 4, pp. 1004–1014, Dec. 2019, doi: 10.1109/TTE.2019.2927803.

[15] Y. Lim, H. Tang, S. Lim, and J. Park, "An adaptive impedance-matching network based on a novel capacitor matrix for wireless power transfer," *IEEE Trans. Power Electron.*, vol. 29, no. 8, pp. 4403–4413, Aug. 2014, doi: 10.1109/TPEL.2013.2292596.

[16] Z. H. Shi, X. Y. Chen, and Z. C. Qiu, "Modeling of mutual inductance between superconducting pancake coils used in wireless power transfer (WPT) systems," *IEEE Trans. Appl. Supercond.*, vol. 29, no. 2, pp. 1–4, Mar. 2019, doi: 10.1109/TASC.2019.2891682.

[17] G. Lee, B. H. Waters, Y. G. Shin, J. R. Smith, and W. S. Park, "A reconfigurable resonant coil for range adaptation wireless power transfer," *IEEE Trans. Microw. Theory Techn.*, vol. 64, no. 2, pp. 624–632, Feb. 2016, doi: 10.1109/TMTT.2015.2510623.

[18] H. Zeng and F. Z. Peng, "Non-linear capacitor based variable capacitor for self-tuning resonant converter in wireless power transfer," *IEEE Appl. Power Electron. Conf. Expo. (APEC)*, San Antonio, TX, USA, Mar. 2018, pp. 1375–1379, doi: 10.1109/APEC.2018.8341196.

[19] T. Sasatani, Y. Narusue, Y. Kawahara, and T. Asami, "DC-based impedance tuning method using magnetic saturation for wireless power transfer," in *Proc. IEEE Wireless Power Transf. Conf. (WPTC)*, Taipei, Taiwan, Apr. 2017, pp. 1–4, doi: 10.1109/WPT.2017.7953900.

[20] X. Wang and A. Mortazawi, "Bandwidth enhancement of RF resonators using duffing nonlinear resonance for wireless power applications," *IEEE Trans. Microw. Theory Techn.*, vol. 64, no. 11, pp. 3695–3702, Nov. 2016, doi: 10.1109/TMTT.2016.2603984.

[21] O. Abdelatty, X. Wang, and A. Mortazawi, "Position-insensitive wireless power transfer based on nonlinear resonant circuits," *IEEE Trans. Microw. Theory Techn.*, vol. 67, no. 9, pp. 3844–3855, Sep. 2019, doi: 10.1109/TMTT.2019.2904233.

[22] J. Zhou, B. Zhang, G. Liu, and D. Qiu, "Resonance and distance insensitive wireless power. Transfer with parity-time symmetric duffing resonators," in *Proc. IEEE Wireless Power Transf. Conf. (WPTC)*, Montreal, QC, Canada, Jun. 2018, pp. 1–4, doi: 10.1109/WPT.2018.8639115.

[23] J. Fan and D. Li, "A stable nonlinear wireless power transfer system with variable coupling coefficient," China Patent ZL 2019 2 2 270 285.1, Dec. 12, 2019.

[24] S. S. Rao, X. Li, and M. Zhang, "Nonlinear vibration," in *Mechanical Viration*, 4nd ed. Beijing, China: Tsinghua Univ. Press, 2009, pp. 587–635.

[25] Y. Jia, "Review of nonlinear vibration energy harvesting: Duffing, bistability, parametric, stochastic and others," *J. Intell. Mater. Syst. Struct.*, vol. 31, no. 7, pp. 921–944, Feb. 2020, doi: 10.1177/1045389X20905989.

[26] D. Chen, Y. Wang, X. Chen, W. Huang, and J. Xie, "Duffing nonlinearity localization via extension energy confinement in an elastic mode semicircular beams resonator," *IEEE Electron Device Lett.*, vol. 40, no. 2, pp. 314–317, Feb. 2019, doi: 10.1109/LED.2018.2889468.

[27] A. Chowdhury, M. G. Clerc, S. Barbay, I. Robert-Philip, and R. Braive, "Weak signal enhancement by nonlinear resonance control in a forced nano-electromechanical resonator," *Nature Commun.*, vol. 11, no. 1, pp. 2400–2408, May 2020, doi: 10.1038/s41467-020-15827-3.

[28] Z.-P. Jiang, "Advanced feedback control of the chaotic duffing equation," *IEEE Trans. Circuits Syst. I, Fundam. Theory Appl.*, vol. 49, no. 2, pp. 244–249, Feb. 2002, doi: 10.1109/81.983872.

[29] H. Vahedi, G. B. Gharehpetian, and M. Karrari, "Application of duffing oscillators for passive islanding detection of inverter-based distributed generation units," *IEEE Trans. Power Del.*, vol. 27, no. 4, pp. 1973–1983, Oct. 2012, doi: 10.1109/TPWRD.2012.2212251.

[30] V. B. Haas, "On the frequency response of a van der pol-duffing oscillator," *Proc. IEEE*, vol. 59, no. 2, pp. 334–335, Feb. 1971, doi: 10.1109/PROC.1971.8171.

[31] I. Kovacic and M. J. Brennan, "Free vibration of a Duffing oscillator with viscous damping," in *The Duffing Equation: Nonlinear Oscillators and Their Behaviour*. Hoboken, NJ, USA: Wiley, 2011, pp. 55–80, doi: 10.1002/9780470977859.

[32] D. Jordan and P. Smith, "Second-order differential equations in the phase plane," in *Nonlinear Ordinary Differential Equations: Problems and Solutions*. Oxford, U.K.: Oxford Univ. Press, 2007, pp. 1–62.

XU YANG received the B.Sc. degree from the School of Electrical and Electronic Engineering, Changchun University of Technology, Jilin, China, in 2010, and the M.Sc. degree in electrical engineering from Henan Polytechnic University, Henan, China, in 2013. He is currently pursuing the Ph.D. degree with the School of Electrical Engineering, Beijing Jiaotong University, Beijing, China. His research interests include wireless power transfer and power electronic converters.

CHAOQUN JIAO received the M.Sc. and Ph.D. degrees in electrical theory and new technology from North China Electric Power University, Hebei, China, in 2003 and 2006, respectively. Since 2006, he has been working with the School of Electrical Engineering, Beijing Jiaotong University. His research interests include electrical theory and new technology, ultra high-voltage technology, and wireless power transfer.

JUNFENG YANG received the B.S. degree in electrical engineering from Beijing Jiaotong University, Beijing, China, in 2012, where he is currently pursuing the Ph.D. degree in electrical engineering. His research interests include power electronics and wireless power transfer.

JING FAN received the B.Sc. degree from the Department of Physics, Henan Normal University, China, in 1997, the M.Sc. degree from the School of Information Science and Engineering, East China University of Science and Technology, Shanghai, China, in 2005, and the Ph.D. degree from the School of Mechanical Electric and Information Engineering, China University of Mining and Technology, Beijing, China, in 2011. He is currently a Professor with the School of Information Engineering, Nanyang Institute of Technology, Nanyang, China. His research interests include wireless power transfer, electromagnetic field propagation in mine tunnels, and environmental energy harvesting.

DINGZHEN LI received the B.Sc. degree from the Department of Automatic Control, Yanshan University, Qinhuangdao, China, in 1996, and the M.Sc. degree from the School of Mechanical Engineering, Nanjing University of Science and Technology, Nanjing, China, in 2007. She is currently a Professor with the School of Information Engineering, Nanyang Institute of Technology, Nanyang, China. Her research interests include wireless power transfer, instrument detection and automatic control, and environmental energy harvesting.

BAO WANG received the B.S. degree in physics from Henan Normal University, Xinxiang, Henan, in 2015, and the Ph.D. degree in optics from the Huazhong University of Science and Technology, in 2019. He is currently a University Lecturer with the Nanyang Institute of Technology. His research interests include quantum optics, cavity optomechanics, nonlinear optics, coherent phenomena, and chaos.